ORNL/SUB-4269/4

THERMO/VISCOELASTIC ANALYSIS OF THE WASTE-CONTAINER SLEEVE: I. TIME-DEPENDENT SALT LOADING ON THE SLEEVE AND CLOSURE OF THE DRILLHOLE

Technical Memorandum Report RSI-0020

Gary D. Callahan
Joe L. Ratigan

October 31, 1975

This report was prepared by RE/SPEC, Inc. under Subcontract 4269 with Union Carbide Corporation, Nuclear Division. The subcontract was administered by Oak Ridge National Laboratory

UNION CARBIDE
OFFICE OF WASTE ISOLATION
OAK RIDGE, TENNESSEE

prepared for the **U.S. ENERGY RESEARCH AND DEVELOPMENT ADMINISTRATION**
under **U.S. GOVERNMENT** *Contract W-7405 eng 26*

TECHNICAL MEMORANDUM REPORT RSI-0020

THERMO/VISCOELASTIC ANALYSIS OF THE WASTE-CONTAINER SLEEVE:

I. TIME-DEPENDENT SALT LOADING ON THE SLEEVE AND CLOSURE OF THE DRILLHOLE

Submitted To

Holifield National Laboratory
Oak Ridge, Tennessee

operated by

Union Carbide Corporation
Nuclear Division
for the
Energy Research and Development Administration

by

Gary D. Callahan
Joe L. Ratigan

RE/SPEC INC.
P. O. BOX 725 - RAPID CITY, S. D. 57701 - 605/343-7868

ORNL-SUB-4269-4

TECHNICAL MEMORANDUM REPORT RSI-0020

THERMO/VISCOELASTIC ANALYSIS OF THE WASTE-CONTAINER SLEEVE:

I. TIME-DEPENDENT SALT LOADING ON THE SLEEVE AND CLOSURE OF THE DRILLHOLE

Submitted To

Holifield National Laboratory
Oak Ridge, Tennessee

operated by

Union Carbide Corporation
Nuclear Division
for the
Energy Research and Development Administration

by

Gary D. Callahan
Joe L. Ratigan

of

RE/SPEC Inc.
Rapid City, SD 57701

October 31, 1975

TABLE OF CONTENTS

FOREWORD

The technical content of this report has been reviewed by Dr. Arlo F. Fossum, Dr. James E. Russell and Dr. Paul F. Gnirk.

LIST OF FIGURES

LIST OF FIGURES (CONT'D)

LIST OF TABLES

RE/SPEC INC.

P. O. Box 725 • Rapid City, S D 57701 • 605/343-7808

October 31, 1975

TECHNICAL MEMORANDUM REPORT RSI-0020

TO: Dr. William C. McClain
Holifield National Laboratory
P. O. Box Y
Oak Ridge, TN 37830

FROM: Gary D. Callahan
Joe L. Ratigan
RE/SPEC Inc.
P. O. Box 725
Rapid City, SD 57701

SUBJECT: Thermo/Viscoelastic Analysis of the Waste-Container Sleeve: I. Time-Dependent Salt Loading on the Sleeve and Closure of the Drillhole (Union Carbide Corporation, Nuclear Division Subcontract No. 4269; RSI/001000/FY75).

1. INTRODUCTORY REMARKS

Canister retrievability and encasement-sleeve structural integrity questions have led to detailed analyses of the canister/drillhole region (near field) for high-level waste burial in salt. Past studies have been concerned with maximum (upper bound) stresses that could be developed on and within the sleeve as a result of various boundary conditions at the sleeve-salt interface. The objective of this report is to present estimates of the radial sleeve loading and drillhole closure resulting from thermo/viscoelastic behavior of the salt. Two cases are considered, namely: (a) fixing of the drillhole surface against radial displacement, and (b) allowing the drillhole to displace radially without restraint. In case (a), however, the drillhole is allowed to displace elastically before being fixed against further radial movement. In effect, the computer code excavates the drillhole (21 inches in diameter and 18 feet in length), which is centrally located in the room floor, and emplaces the steel sleeve,

which acts as a rigid inclusion and rests on the bottom of the drillhole. Subsequently, the heat source is activated after approximately one week of simulated time, representing emplacement of the waste canister (10 feet in length) within the lower section of the sleeve.

Use was made of the SALT-3A finite element model, as shown in Figure 1.1 which was developed in axially symmetric r-z geometry according to the room, pillar, waste container, and drillhole dimensions appropriate for the New Mexico pilot-plant repository concept. In particular, the model contains 317 nodes and 542 elements and represents a 202 foot vertical section through the room and pillar level. The floor level of the 18 by 18 foot room is located at a depth of 2,000 feet. The pillar width is 60 feet with the midpoint of the rib at the 1,991 foot level. The thermoelastic material properties used in the SALT-3A model are summarized in Table 1.1, and the creep law is given in Section 4. For the stress analysis, the material in the 18 foot drillhole was given properties of air. Whereas, in the temperature analysis, only the upper eight foot of the drillhole was considered to be air, with the lower ten foot being the heat generating waste. This type of material identification resulted in the appropriate temperature fields and allowed unrestricted displacement of the drillhole wall.

TABLE 1.1

Material Properties of Salt and the Waste Container Arrangement

Material	Elastic Moduli		γ pfc	Thermal Properties		
	$E \times 10^6$ psi	ν		k Btu/Hr-Ft-^oF	$\alpha \times 10^{-6}$ in./in./^oF	Heat Generation Rate (KW)
Salt	0.8	0.4	135	2.43	22.22	-
Waste	0.4	0.38	113	0.25	-	5

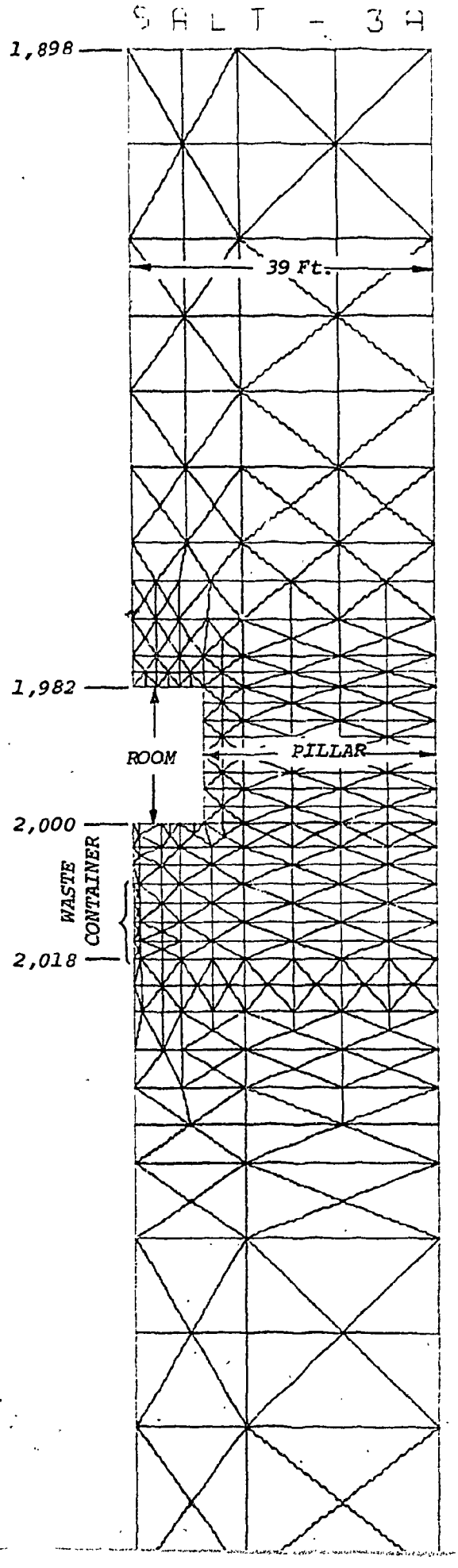

ROOM HEIGHT = 18 FT.
ROOM WIDTH (HALF) = 9 FT.
PILLAR WIDTH (HALF) = 30 FT.
LENGTH OF DRILLHOLE = 18 FT.
LENGTH OF WASTE CONTAINER = 10 FT.
DIAMETER OF DRILLHOLE = 21 IN.
NO. OF ELEMENTS = 542
NO. OF NODES = 317

Figure 1.1. Finite Element Mesh of the SALT-3A Repository Model.

Premining stresses are computed according to the overburden gravity loading neglecting any excavation. The elastic solution provides the post-mining stress state based on the initial gravity loading.

The thermo/viscoelastic analyses, assuming that the viscous behavior is time and stress dependent only (see Appendix A for a discussion of viscoelasticity), predicts a maximum drillhole surface pressure of approximately 3,000 psi after one-half year of heating, assuming the drillhole surface is fixed against radial displacement. With the drillhole surface free to displace radially, the radial displacement is observed to be about 1.5 inches after twenty-five years of heating, for a total drillhole closure of 3.0 inches. In this particular case, with the centerline of the pillar being a line of symmetry, the material expansion upon heating forces the salt upward and into the room and drillhole areas.

2. THERMO/VISCOELASTIC ANALYSIS OF SALT LOADING ON THE DRILLHOLE SURFACE

As previously mentioned, the computer code simulates excavation of the drillhole in the room floor and determines the state of stress as a consequence of the initial gravity load (assuming an overburden density of 142.5 pcf) in the salt formation. Subsequently, the drillhole is fixed against radial displacement providing a maximum or upper bound situation. Since the stiffness of the steel sleeve surrounding the waste canister is greater than that of the salt, the rigid boundary seems realistic. This condition (i.e. rollers along the drillhole) implies that a perfect slip condition exists at the sleeve-salt interface.

The post-mining stress state is utilized for the initiation of the viscous behavior of the salt. Emplacement of the waste container and, consequently, the initiation of the thermal effects may be delayed for a prescribed time interval. In this particular case, a delay of one week was arbitrarily chosen. The creep law utilized is based on experimental results of block salt under conditions of confining pressure and room temperature as previously reported (2,3).

A model of an underground configuration in r-z geometry may be difficult to visualize when one considers an infinite row of rooms and pillars. As shown in Figure 2.1, lines of symmetry may be taken through the center of the room and the center of the pillar. Section A-A in Figure 2.1 shows a typical model which may be taken in either x-y or r-z geometry. Neither model in itself will provide the detail needed for an analysis of the area around the room and pillar and the drillhole. The two dimensional x-y model sufficiently represents the room and pillar, but lacks the ability to model the drillhole area in detail. Conversely, the axially symmetric r-z model represents the drillhole area in detail, but sacrifices accurate modeling of the room and pillar. For these particular reasons, a combination of the aforementioned procedures has been utilized in the past. Since this investigation is concerned with the sleeve loading and drillhole closure, the axially symmetric r-z model has been utilized to obtain the needed detail about the drillhole. The r-z geometry will provide results in the room and pillar comparable to the x-y analysis until the boundary effects become important. Considerations of stress and displacement behavior about the room and pillar will be the subject of the second report in this memoranda series.

Radial compressive loading of the salt on the sleeve, as compared with the temperature rise, is shown in Figure 2.2. After the initiation of heating,

the radial pressure along the sleeve salt interface increases quite rapidly due to the localized heating and a large thermal gradient. A maximum horizontal pressure of approximately 3,000 psi near the base of the sleeve is predicted after one-half year of heating. Subsequently, the temperature field progresses outward from the waste container and the thermal gradients become less severe, resulting in a decrease in the radial stress.

The radial stress distribution at the level of the canister midpoint at various times is displayed in Figure 2.3. As shown in the figure, the radial stress at the sleeve-salt interface reaches a maximum at approximately one-half year; conversely, the radial stress at the centerline of the pillar attains a maximum value in about ten years.

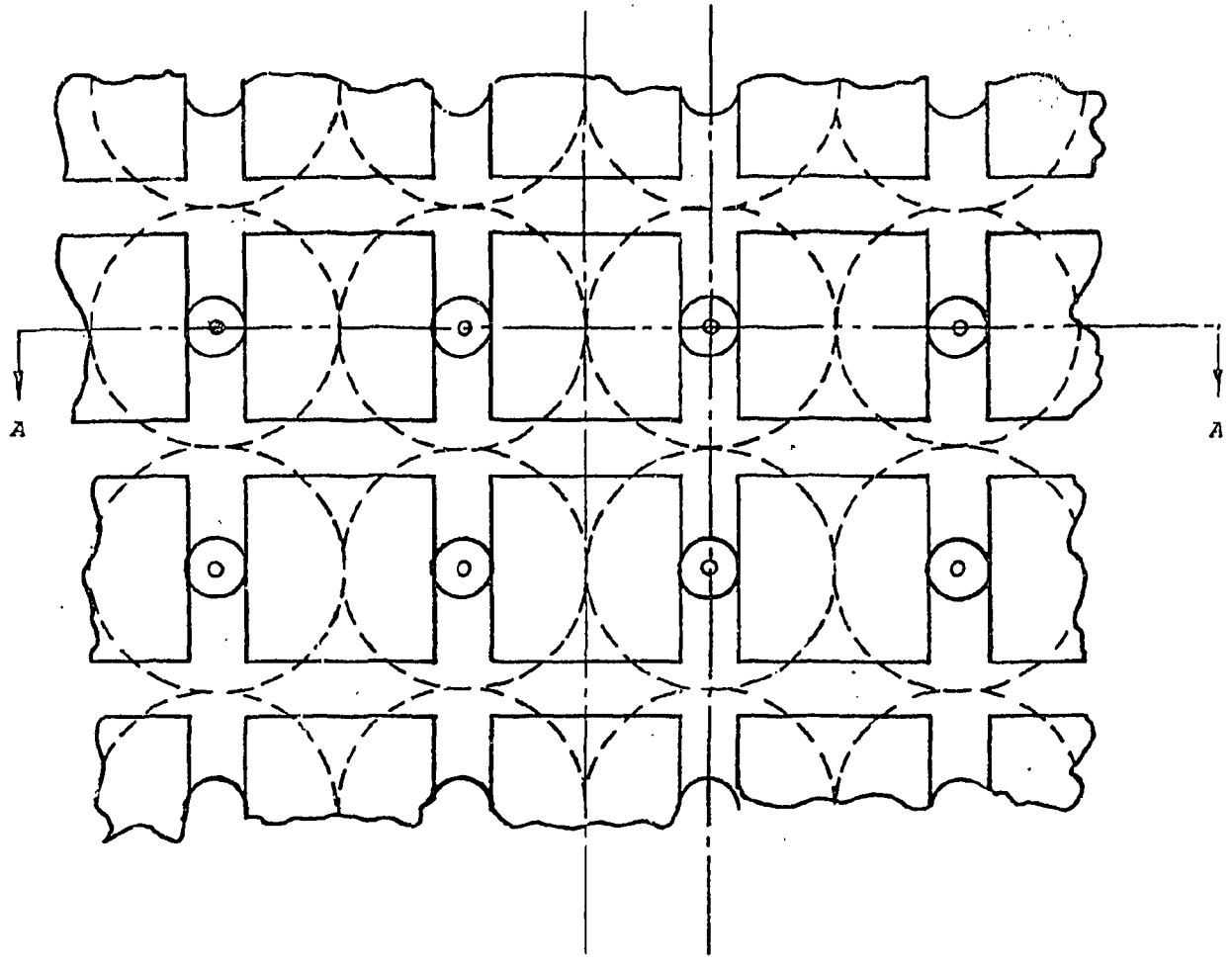

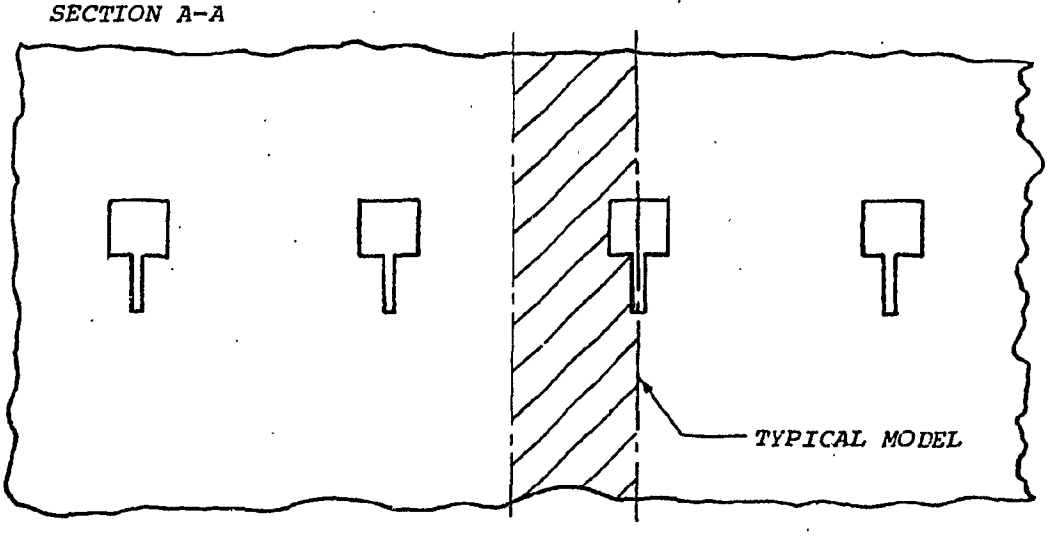

Figure 2.1. Two dimensional representation of infinite rows of rooms and pillars in r-z and x-y geometry.

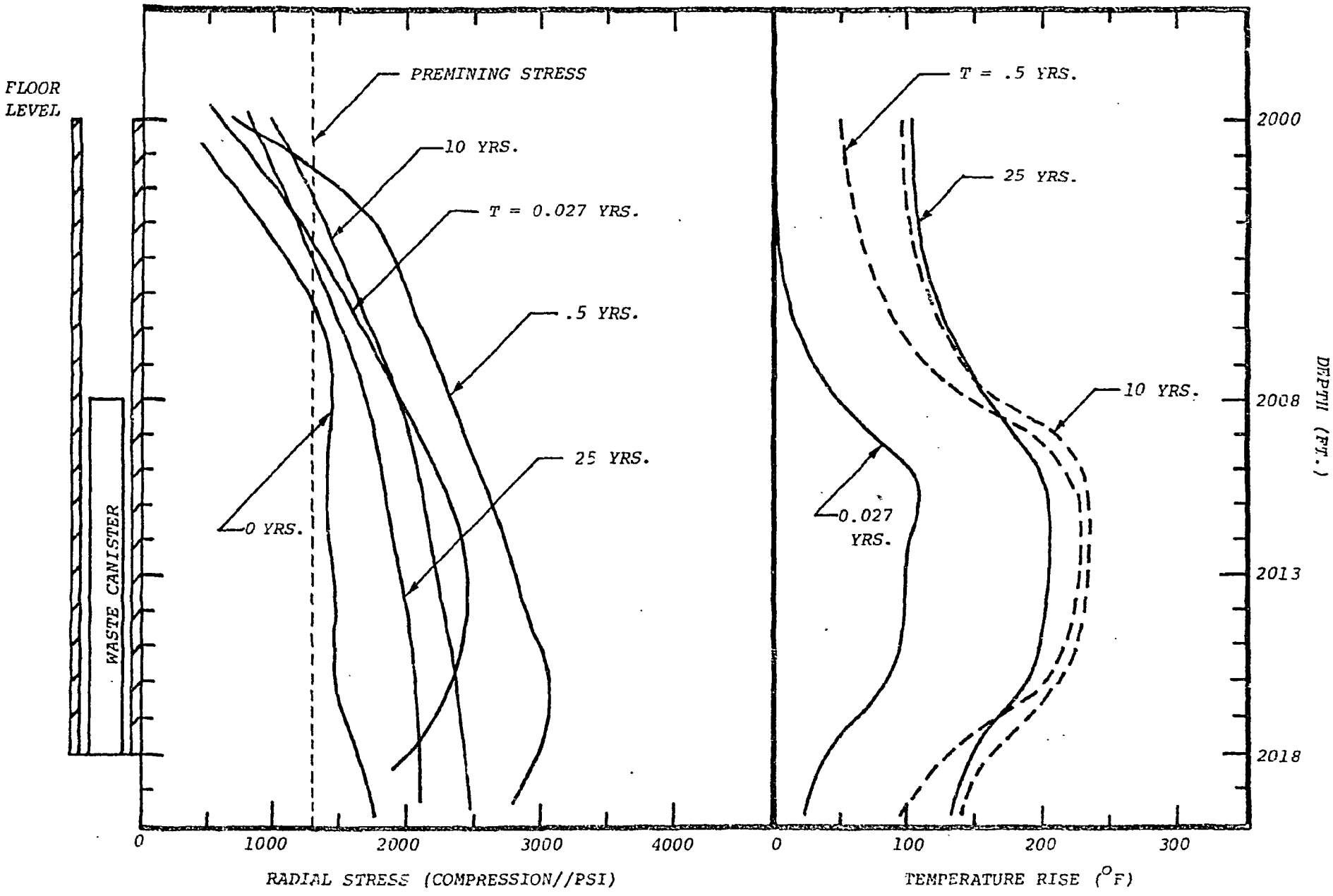

Figure 2.2. Thermo/Viscoelastic Behavior of Radial Stress Compared with Temperature Rise Along Sleeve-Salt Interface (Drillhole Restricted Radially).

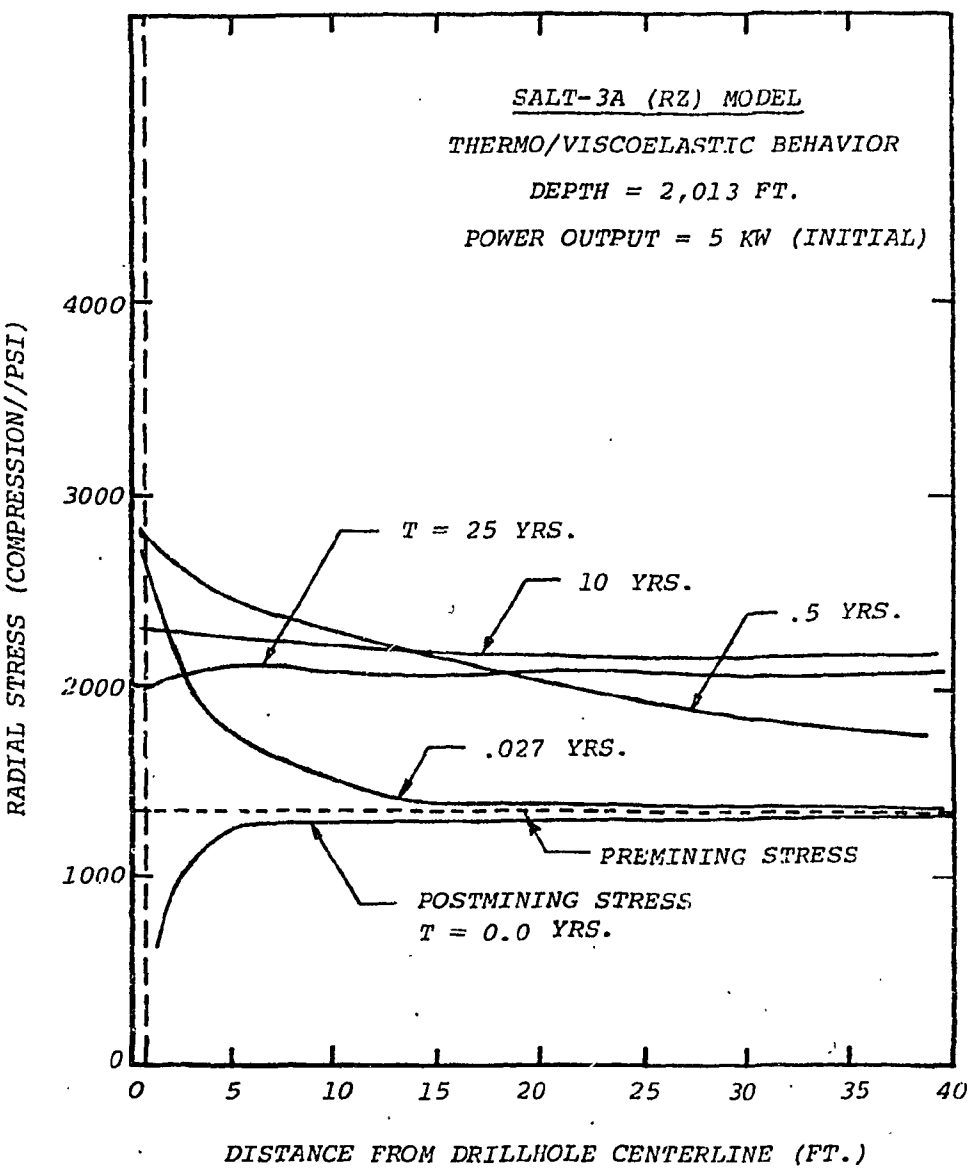

Figure 2.3. Radial Stress Distribution Around the Drillhole at 2,013 Feet (Radial Drillhole Movement Restricted).

3. THERMO/VISCOELASTIC ANALYSIS OF DRILLHOLE CLOSURE

Canister retrievability and encasement sleeve questions require an assessment of closure of the drillhole centrally located in a typical repository room. Initially providing an airgap between the salt and sleeve would possibly reduce the radial loading on the sleeve, maintain the structural integrity of the sleeve, and ensure canister retrievability. The airgap design, however, should be considered jointly with a structural analysis of the floor. An array of enlarged drillholes could conceivably defeat the purpose of the airgap if excessive amounts of material had to be removed.

The objective of this analysis is to provide insight into the varying methods for emplacement of the waste container by identifying anticipated magnitudes of drillhole closure. The closure data was obtained utilizing the SALT-3A r-z finite element model (Figure 1.1). The drillhole surface was allowed to displace freely in the radial direction by 'filling' the drillhole with air elements which experienced the same temperatures as the waste but offered no resistance to closure. Assuming that the initial elastic displacements are instantaneous and negligible in comparison with those resulting from the thermal and viscous behavior, the displacement fields presented herewith consist of only the cumulative thermal and viscous displacements.

The thermo/viscoelastic radial displacements at a depth of 2,013 feet (midpoint of waste container) are illustrated in Figure 3.1 for a condition in which the radial displacement of the drillhole surface is unrestricted. Results as calculated 3.5 feet from the centerline of the drillhole are also presented for comparison. The displacement pattern shows the surface bowing inward during the early time period due to localized heating in the canister area. The drillhole surface continues to move inward with time, due to viscous behavior and thermal expansion of the salt, to a maximum value of approximately 1.5 inches, for a total diametrical closure of 3.0 inches (about 14% of the original drillhole diameter) after 25 years. At a radial distance of 3.5 feet from the centerline of the drillhole, an expansion of the salt is observed during the early time period. Since the centerline of the pillar is a line of symmetry, further outward expansion of the salt with continued heating is seen to cease, and an inward movement is observed. This phenomenon results in drillhole closure when considering the drillhole surface free, or increased radial loading when considering the surface fixed.

Figure 3.2 illustrates the vertical displacements observed for points along the drillhole surface up to the floor of the room. An upward, rigid body type motion is observed as the salt expands when heated. During early time periods, the boundary restrictions on the drillhole surface are of no consequence as regards the displacement field. However, as heating continues with the salt contained (i.e. drillhole fixed against radial movement) an increase in the uplift is observed.

The relative difference in vertical displacements across the model, at a depth of 2,013 feet (midpoint of the waste container), is shown in Figure 3.3. The maximum difference traversing from the drillhole surface to the centerline of the pillar is approximately one inch. At this particular depth, the vertical displacements are essentially the same for the boundary conditions on the drillhole surface of totally restricted and unrestricted radial displacement.

Considering the displacement results, one can conclude that the viscous behavior is dominate during the very early time periods. Shortly after heating is initiated, the thermal effects become important and tend to dominate for a long period of time due to the large thermal expansion coefficient of salt. Once the temperature field peaks and starts to decline, the trend reverses and the viscous behavior becomes increasingly more important.

The thermal boundary conditions become significant as regards vertical displacements when long time periods are under consideration. The upper boundary, generally taken at constant temperature, will result in a large amount of heat removal if the temperature rise in this area is significant. The lower boundary, generally assumed to be insulated, will result in temperatures too large if the boundary is not sufficiently removed from the heat source. For the SALT-3A Model, the temperature rise at the lower boundary was approximately $80^{o}F$ after twenty-five years. The magnitude of the temperature rise indicates that the model is becoming inadequate for this period of time. However, the results do offer an upper bound by predicting greater thermal expansion provided by the magnitude of the temperature field at the boundary.

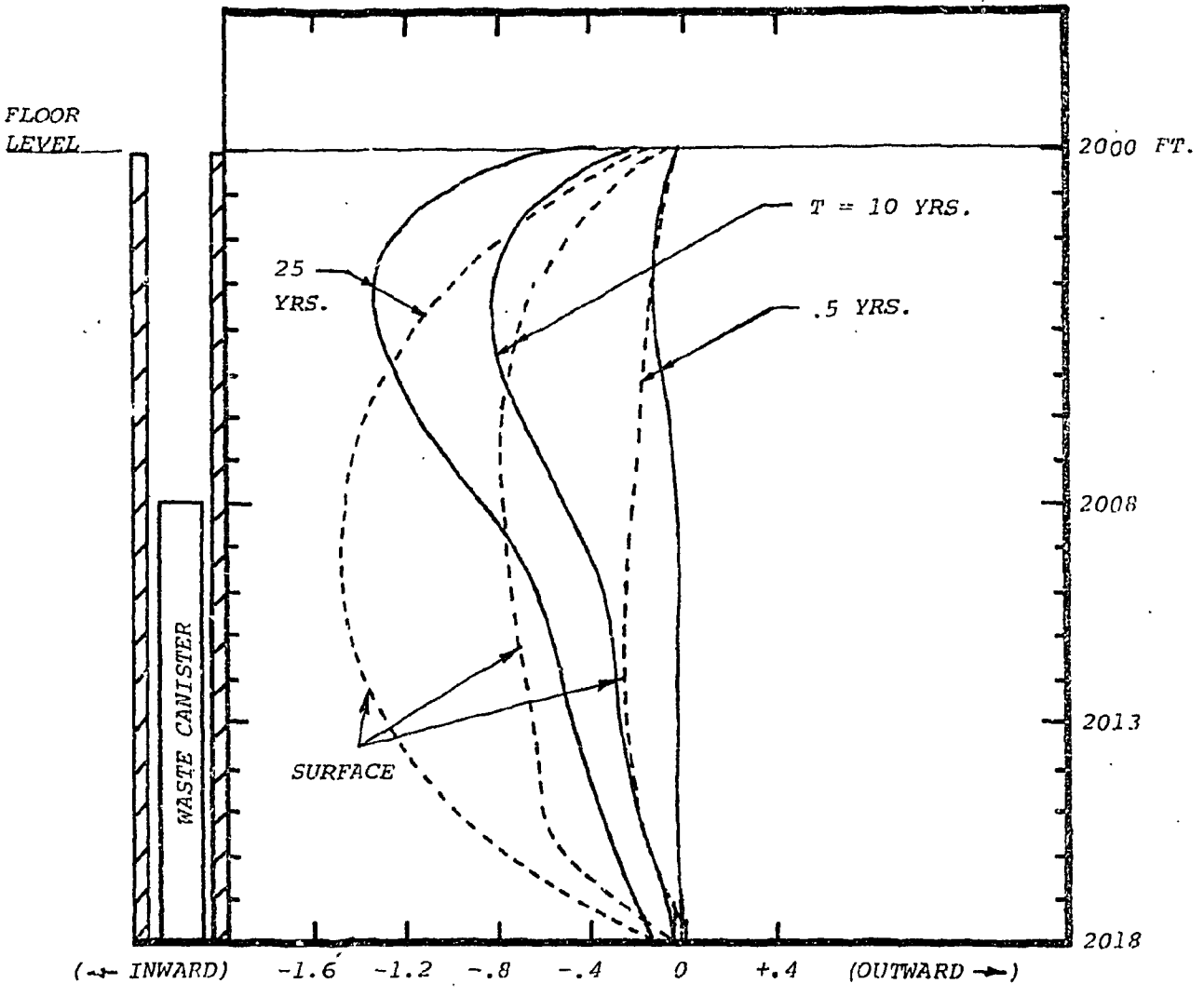

Figure 3.1. Thermo/Viscoelastic Radial Displacements at the Surface of the Drillhole and 3.5 Feet from the Centerline of the Waste Canister for the Drillhole Surface Free (+ Outward)

NOTE: Displacements are 3.5 Feet from the Drillhole Surface Unless Labeled Surface

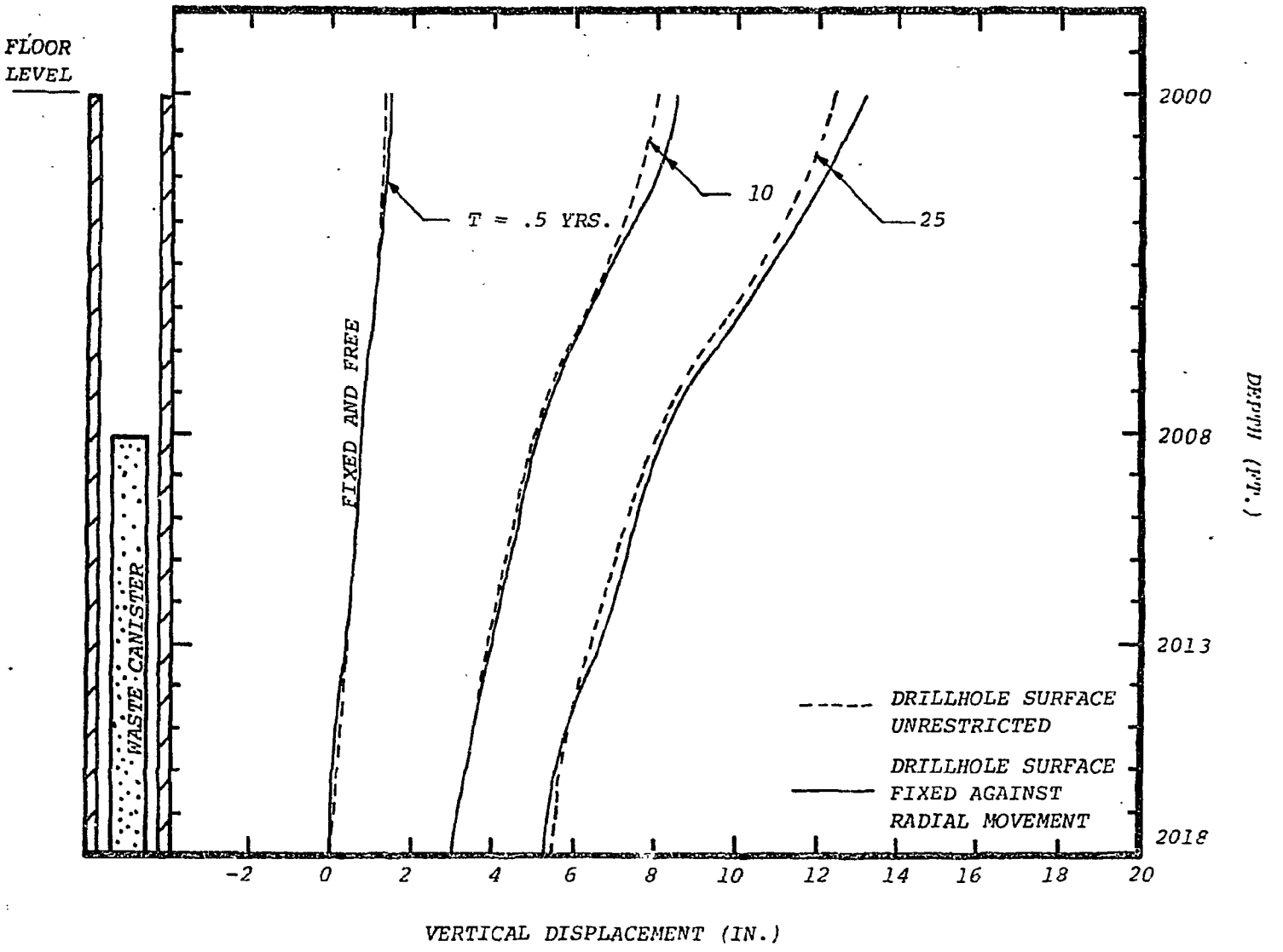

Figure 3.2. Thermo/Viscoelastic Vertical Displacements Along the Sleeve-Salt Interface (+ Upward).

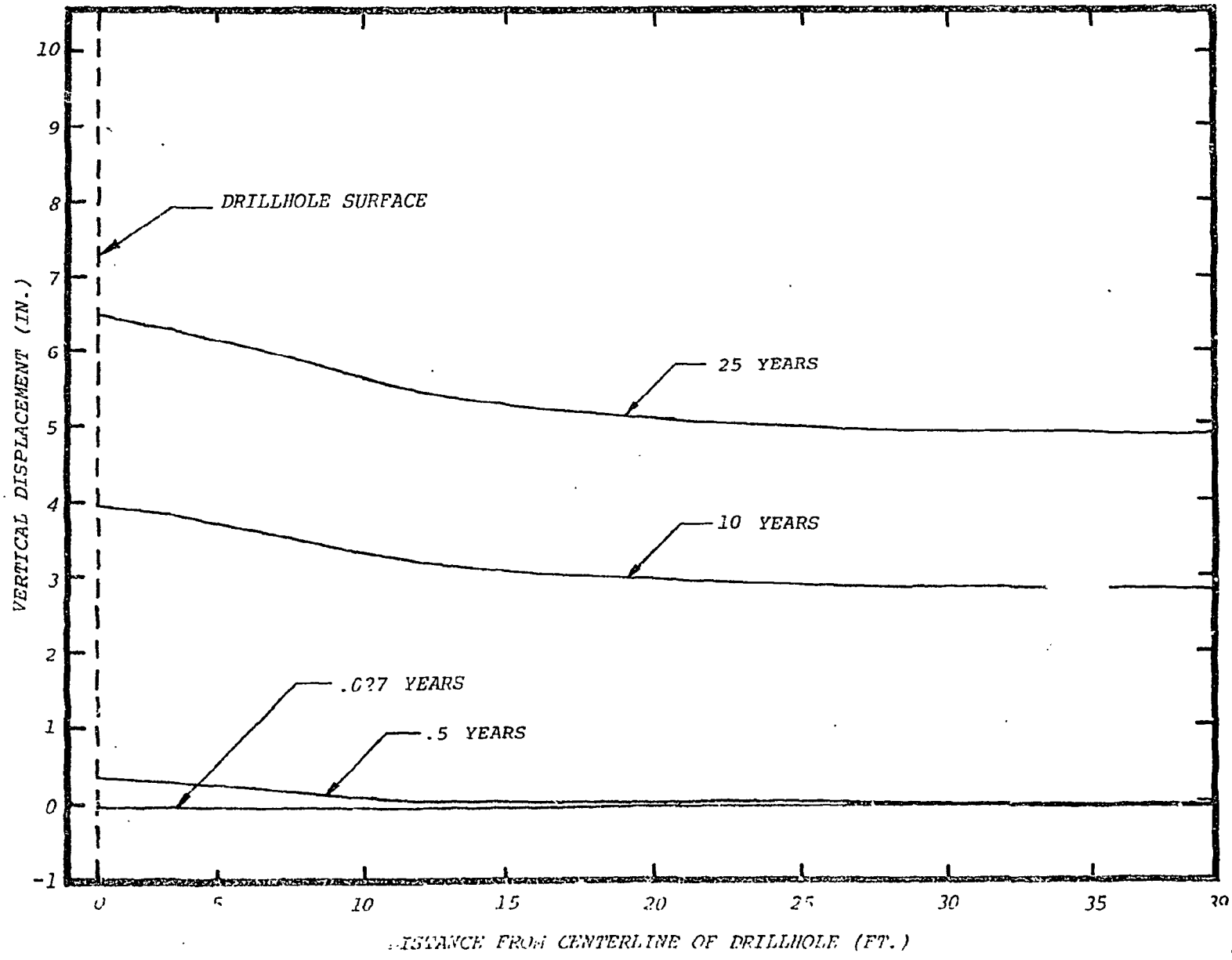

Figure 3.3. Thermo/Viscoelastic Displacements at a Depth of 2,013 Feet and Across the Model from the Drillhole Surface to the Centerline of the Pillar (+ Upward).

4. DRILLHOLE CREEP CLOSURE UNDER CONSTANT STRESS CONDITIONS

Problems involving stress fields independent of material properties may be solved without resorting to the usual incremental type procedures provided that the materials are time hardening only. This type of problem includes statically determinate problems and problems where stresses are independent of material properties (plane elasticity problems having only stress boundary conditions and no body forces). Generally the elastic stress field around an underground opening does not fall into this class since horizontal displacement boundary conditions are specified on the vertical boundaries of the model. These boundary conditions give the premining horizontal stress, σ_H, as

$$\sigma_H = \frac{\nu}{1-\nu}\sigma_v$$

where ν is Poisson's ratio and σ_v is the vertical premining stress.

The creep law, as based on experimental evidence (2,3), may be written in incremental form as:

$$\Delta\varepsilon^c_{ij} = \frac{3}{4}\left[\frac{\sigma_e}{24,300}\right]^3 \frac{\Delta t}{\sqrt{t}}\left[\frac{S_{ij}}{\sigma_e}\right] \qquad (i,j = 1,2,3)$$

$\Delta\varepsilon^c_{ij}$ = incremental creep strain components

σ_e = effective stress = $\sqrt{\tfrac{1}{2}\{(\sigma_1-\sigma_2)^2+(\sigma_2-\sigma_3)^2+(\sigma_3-\sigma_1)^2\}}$ (psi)

S_{ij} = deviatoric stress components = $\sigma_{ij}-\frac{1}{3}\delta_{ij}\sigma_{kk}$ (psi)

t = total time (hrs)

Δt = incremental time (hrs.)

By use of this creep law and an assumption of a time-independent stress state around the drillhole, an <u>upper bound</u> on the magnitude of the creep displacements may be obtained. The appropriate equation can be formulated by noting that the force components corresponding to the incremental (creep) displacements at time $t_i = i\Delta t$ may be written as a summation of the incremental displacements.

$$\delta_n = C \sum_{i=1}^{i=n} \frac{\Delta t}{\sqrt{t_i}}$$

where C is a proportionality coefficient. In the limit as $\Delta t \to 0$ and $n \to \infty$

$$\delta(t) = C \int_0^t \frac{dt}{\sqrt{t}} = C\ 2\ \sqrt{t}$$

To evaluate C, let $t = t_1$, then

$$\delta(t_1) = \delta_1 = C\ 2\ \sqrt{t_1}$$

and

$$C = \frac{\delta_1}{2\ \sqrt{t_1}}$$

Therefore,

$$\delta(t) = \delta_1 \sqrt{\frac{t}{t_1}}$$

and the displacement at any time, $\delta(t)$, may be predicted utilizing the displacement δ_1 at time t_1 from the finite element method results.

The above discussed method was followed using the axially symmetric r-z finite element model SALT-10A shown in Figure 4.1. SALT-10A models the area around the drillhole and below the floor of the room. Body forces were neglected and radial pressures equivalent to the premining horizontal stress (1324 psi) and lithostatic stress (2000 psi) were applied to the outer boundary. The resulting viscous displacements from this model were then used to predict the drillhole closures at advanced time periods.

The premining horizontal stress resulted in an inward displacement of approximately 3×10^{-4} inches at 2.5×10^{-6} years, which projects an inward displacement of 0.95 inches at twenty-five years for a total diametrical drillhole closure of 1.9 inches. The lithostatic loading resulted in an inward displacement of approximately 1×10^{-3} inches at 2.5×10^{-6} years which projects an inward displacement of 3.2 inches at twenty-five years, for a total diametrical drillhole closure of 6.4 inches.

The actual radial loading which would be perceived about an underground opening is probably somewhere between the premining and the lithostatic stress states. Therefore, an average of the two loading conditions or 4 inches of diametrical closure would probably be a good upper bound estimate.

This method of viscous closure prediction must be viewed as an upper bound since a constant stress state is specified and only time hardening is considered.

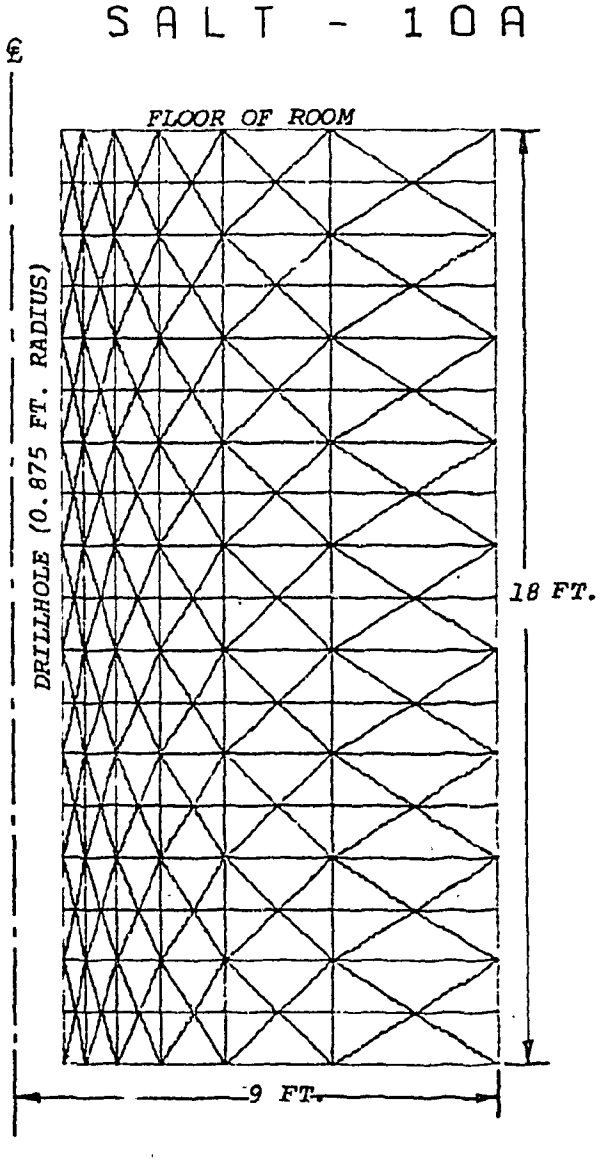

Figure 4.1. Finite Element Mesh Used for Creep Closure Predictions Under Constant Stress Conditions.

REFERENCES

1. Timoshenko and Goodier: Theory of Elasticity, McGraw-Hill, (1970).

2. Gnirk, P. F., Pariseau, W. G., Russell, J. E., Wawersik, W. R., Callahan, G. D., and Hovland, H.: "Analysis and Evaluation of the Rock Mechanics Aspects of the Proposed Salt Mine Repository", Summary Progress Report (RSI-0005), Prepared for the Oak Ridge National Laboratory (Union Carbide Corp., Nuclear Division Subcontract No. 3706), Sept. 1973.

3. Gnirk, P. F., Callahan, G. D., Pariseau, W. G., Van Sambeek, L. L., and Wawersik, W. R.: "Analysis and Evaluation of the Rock Mechanics Aspects of the Proposed Salt Mine Repository Concept III", Summary Progress Report (RSI-0012), Prepared for the Oak Ridge National Laboratory (Union Carbide Corp., Nuclear Division Subcontract No. 3706), Sept. 1974.

4. Christensen, R. M.: Theory of Viscoelasticity, Academic Press, New York, (1971).

5. Jaeger, J. C. and Cook, N.G.W.: Fundamentals of Rock Mechanics, Methuen, London, (1969).

6. Zienkiewicz, O. C.: The Finite Element Method, McGraw-Hill, London, (1971).

7. Winkel, B. V.: "Analysis of Time-Dependent Deformations of Openings in Salt Media", Int. J. Rock Mech. and Min. Sci., Vol. 9, pp. 249-260, (1972).

8. Sutherland, W. H.: "AXICRP - Finite Element Computer Code for Creep Analysis of Plane Stress, Plane Strain, and Axisymmetric Bodies", Nuclear Engineering and Design, Vol. 11, pp. 269-285, (1970).

APPENDIX A

LINEAR AND NONLINEAR CREEP

A.1. INTRODUCTION

Viscoelasticity is an idealization of real material behavior that combines aspects of the behavior of elastic solids and viscous fluids. Creep is considered under the general topic of viscoelasticity. A fundamental concept in viscoelasticity is the memory hypothesis that assumes the current value of stress is determined by the current value of strain and the complete past history of strain (4).

The response of viscoelastic materials is often separated into volumetric (or bulk) behavior and deviatoric (or shear) behavior. This separation is convenient since experimental results on many materials, including salt, indicate that the volumetric response remains essentially elastic at moderate hydrostatic pressures while deviatoric response is viscoelastic.

Viscoelastic response may be either linear or nonlinear in nature. Nonlinear viscoelasticity implies that the current value of stress is nonlinearly related to the current value of strain and the strain history. Creep in salt, as well as metal, has been shown experimentally to be nonlinear, while creep in amorphous polymers is generally observed to be linear.

Creep response is generally observed in three phases: primary, secondary, and tertiary. Primary creep is characterized by a decreasing strain rate under constant stress, while secondary or steady-state creep occurs at constant strain rate. Tertiary creep is recognized by an increasing strain rate under constant stress and generally precedes fracture.

Creep properties are often highly sensitive to temperature changes. In the discussion that follows, we assume that the material properties may be temperature dependent, but the temperature field is assumed to be uncoupled from the stress field.

A.2. MATHEMATICAL STATEMENTS OF CREEP LAWS

Constitutive laws for viscoelastic materials may be stated in operator form, as heredity integrals or in empirical forms taken directly from experimental results.

A.2.1. Operator and Heredity Integral Form

The operator form is convenient in linear viscoelasticity where the Laplace transform and the correspondence principle are often used to establish closed form solutions (5). An equivalent approach for linear problems is the heredity integral approach which emphasizes the hypothesis that a viscoelastic material remembers its previous stress history.

Simple rheological models, composed of springs and dashpots, are commonly used in linear viscoelasticity. Two basic building blocks of these models, the Maxwell model and the Kelvin-Voigt model, are shown in Figure A-1, along with their constitutive equations in operator form and in heredity integral form.

Constitutive equations for nonlinear creep may be stated in the heredity integral form, at least for simple materials that satisfy time translation invariance and are in accord with the fading memory hypothesis (4). In terms of a fundamental creep test, the fading memory hypothesis suggests that the current value of strain depends more heavily on the recent history of stress than it does upon the distant past history. The dependence of strain on the previous values of stress is through a weighting function (the creep compliance function), that assigns a continuously decreasing dependence on past events. For the one dimensional creep test, Christensen developed the following form

$$\varepsilon(t) = \int_{-\infty}^{t} J_1(t-\tau)\,\frac{d\sigma(\tau)}{d\tau}\,d\tau$$

$$+ \int_{-\infty}^{t}\int_{-\infty}^{t}\int_{-\infty}^{t} J_3(t-\tau_1,\ t-\tau_2,\ t-\tau_3)\,\frac{d\sigma(\tau_1)}{d\tau_1}\,\frac{d\sigma(\tau_2)}{d\tau_2}\,\frac{d\sigma(\tau_3)}{d\tau_3}\,d\tau_1 d\tau_2 d\tau_3$$

$$+ \cdots \qquad (A\text{-}1)$$

where ε and σ are strain and stress respectively, and $J_i(\ )$ are the creep compliance functions that characterize the material. Only the odd order terms are present in the above expansion to insure the non-negative character of the stored energy function. If the series is truncated after the linear term, the resulting heredity integral form of the constitutive law is identical to that used in linear viscoelasticity where the priniciple of superposition applies.

In the case of a single step creep test, equation (A-1) becomes;

$$\varepsilon(t) = J_1(t)\,\sigma_0 + J_3(t,\ t,\ t)\,\sigma_0^3 \qquad (A\text{-}2)$$

where $\sigma(t) = \sigma_0 H(t)$

and $H(t) = \begin{cases} 0 & t<0 \\ 1 & t>0 \end{cases}$

have been used.

A.2.2. Empirical Form

Creep tests on salt have indicated that creep strain depends on stress cubed in the following manner (2,3):

$$e_1^c = \left[\frac{S_1}{16{,}200}\right]^3 \sqrt{t}$$

where S_1 = axial component of deviatoric stress (psi)

t = time (hrs.)

e_1^c = axial component of deviatoric creep strain

To date we have not attempted to develop a more general form for the creep function J_3, e.g., $J_3(t-t_1,\ t,\ t)$, $J_3(t-t_1,\ t-t_1,\ t)$ etc., as indicated in the heredity integral in equation (A-1). Nevertheless, the results for a single step creep test, that is, the dependence of creep strain on stress cubed, is encouraging.

Empirical creep laws are frequently used, particularly in modeling nonlinear behavior (6). A state variable approach is often taken, where it is assumed that the increment of creep strain in any small time increment

GENERAL LINEAR CREEP LAW

OPERATOR FORM

$$f(D)S_{ij} = 2\,g(D)\,e_{ij} \quad \text{(Deviatoric)} \qquad i,j = 1,2,3$$

$$f_1(D)S = 3\,g_1(D)e \quad \text{(Volumetric)}$$

where S_{ij} and e_{ij} are deviatoric stress and strain components
e = mean normal strain
S = mean normal stress

$$D^r = \frac{d^r}{dt^r}$$

$$f(D) = \sum_{r=o}^{n} a_r D^r; \quad f_1(D) = \sum_{r=o}^{n_1} a_r^1 D^r$$

$$g(D) = \sum_{r=o}^{m} b_r D^r; \quad g_1(D) = \sum_{r=o}^{m_1} b_r^1 D^r$$

a_r, a_r^1, b_r, b_r^1, n, n_1, m and m_1 are constants

HEREDITY INTEGRAL FORM

$$e_{ij} = \int_{-\infty}^{t} J(t-\tau)\,\frac{dS_{ij}}{d\tau}\,d\tau$$

$$e = \int_{-\infty}^{t} J_b(t-\tau)\,\frac{dS}{d\tau}\,d\tau$$

where $J(\,)$ and $J_b(\,)$ are creep compliances for deviatoric and bulk behavior

SIMPLE LINEAR MODELS

MODEL	KELVIN (Transient Creep)	MAXWELL (Steady-State Creep)
	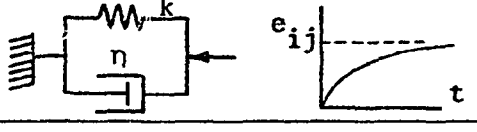	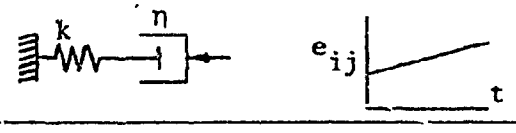
OPERATOR FORM	$(\eta D + k)e_{ij} = S_{ij}$	$De_{ij} = \frac{1}{k} DS_{ij} + \frac{1}{\eta} S_{ij}$
HEREDITY INTEGRAL	$e_{ij} = \int_{-\infty}^{t} J(t-\tau)\frac{dS_{ij}}{d\tau}\,d\tau$; $J(t-\tau) = \frac{1}{k}(\exp(-(t-\tau)/t^*))$ where $t^*=\eta/k$	$e_{ij} = \int_{-\infty}^{t} J(t-\tau)\frac{dS_{ij}}{d\tau}\,d\tau$; $J(t-\tau) = \frac{1}{k}+\frac{t-\tau}{\eta}$
INCREMENT OF CREEP STRAIN	$\Delta e^c_{ij} = De_{ij}\Delta t = (\frac{1}{\eta} S_{ij} - \frac{k}{\nu} e_{ij})\Delta t$	$\Delta e^c_{ij} = De_{ij}\Delta t = \frac{1}{\eta} S_{ij}\Delta t$

Fig. A-1. Linear viscoelastic models.

depends only on the present values of stress and temperature (the state variables), and time. The state variable approach cannot be rigorously developed using modern continuum theory since it appears to ignore the heredity hypothesis. The heredity hypothesis is necessary since a dissipative process such as creep is certainly path dependent and, consequently, it is not possible for strain to depend only on the current values of stress and temperature. However, the state variable approach is in accord with the hypothesis of fading memory that assigns more weight to current values of stress. Furthermore, when using an incremental/computational approach, only the change in strain is required. Apparently, an increment in strain may, in some cases, depend only on stress and temperature; for example, in the simple Maxwell model, the change in strain over a time increment Δt is proportional to the present value of stress:

$$\Delta\varepsilon^c = \frac{d\varepsilon^c}{dt}\,\Delta t = \frac{1}{\eta}\,\sigma\,\Delta t$$

where the stress is assumed to be constant over the time interval.

A.3. FINITE ELEMENT SOLUTION PROCEDURE

A.3.1. Solution Procedure

The thermo/viscoelastic finite-element computer code TEVCO uses the fundamental solution procedure outlined in Appendix B of Summary Progress Report RSI-0005 (2); i.e., an incremental procedure with possible iteration within each increment. This is a general approach to solving nonlinear problems and appears to be widely accepted at this point in time.

A.3.2. Assumptions

Assumptions inherent in the present formulation are given as follows:

(1) The material is assumed to be isotropic with identical properties in tension and compression;

(2) Plastic flow and fracture are not considered;

(3) The solution at $t = 0$ is entirely elastic;

(4) Changes in strain due to temperature fluctuation are considered;

(5) Large displacements are possible;

(6) It is possible to compute $\Delta\varepsilon^c$ for each element in each time increment using previously calculated stresses, strains, and temperatures.

A.3.3. Verification of Solution Procedure and Assumptions

The validity of the incremental approach used in the code has been established by comparison with known results. In order for the code to be valid, it must:

(a) reproduce the strain versus time results from the statically determinate creep tests from which the constitutive law has been developed; and

(b) approach a closed form solution in a statically indeterminate problem where stress components vary with time.

These conditions are necessary for the validity of the code, but not sufficient to demonstrate applicability under all circumstances.

The requirement (a) above is satisfied exactly for the linear Maxwell model. In order to check requirement (b), the problem of a linear Maxwellian half-space creeping from an initial elastic state toward a final lithostatic state has been chosen. The closed form three-dimensional solution is available (see Jaeger and Cook (5), p. 309). After altering the published solution for consistency of notation, the solution is:

σ_v = vertical stress = S = constant (for a particular depth)

σ_H = horizontal stress = $\{1 - \frac{3k(\exp(-t/t_1))}{3K + 2k}\} S$

where $t_1 = \frac{3K + 2k}{3Kk} \eta$

K = bulk modulus

k = elastic spring constant

such that the following constitutive equations are followed

$$\frac{de_{ij}}{dt} = \frac{1}{k} \frac{dS_{ij}}{dt} + \frac{1}{\eta} S_{ij}$$

$$\sigma_m = K\Sigma\varepsilon_{kk}$$

where e_{ij} and S_{ij} are respectively the components of the deviatoric strain and stress tensors, and σ_m is the mean normal stress.

The above closed form solution is compared with the axially symmetric finite-element code solution as shown in Figure A-2.

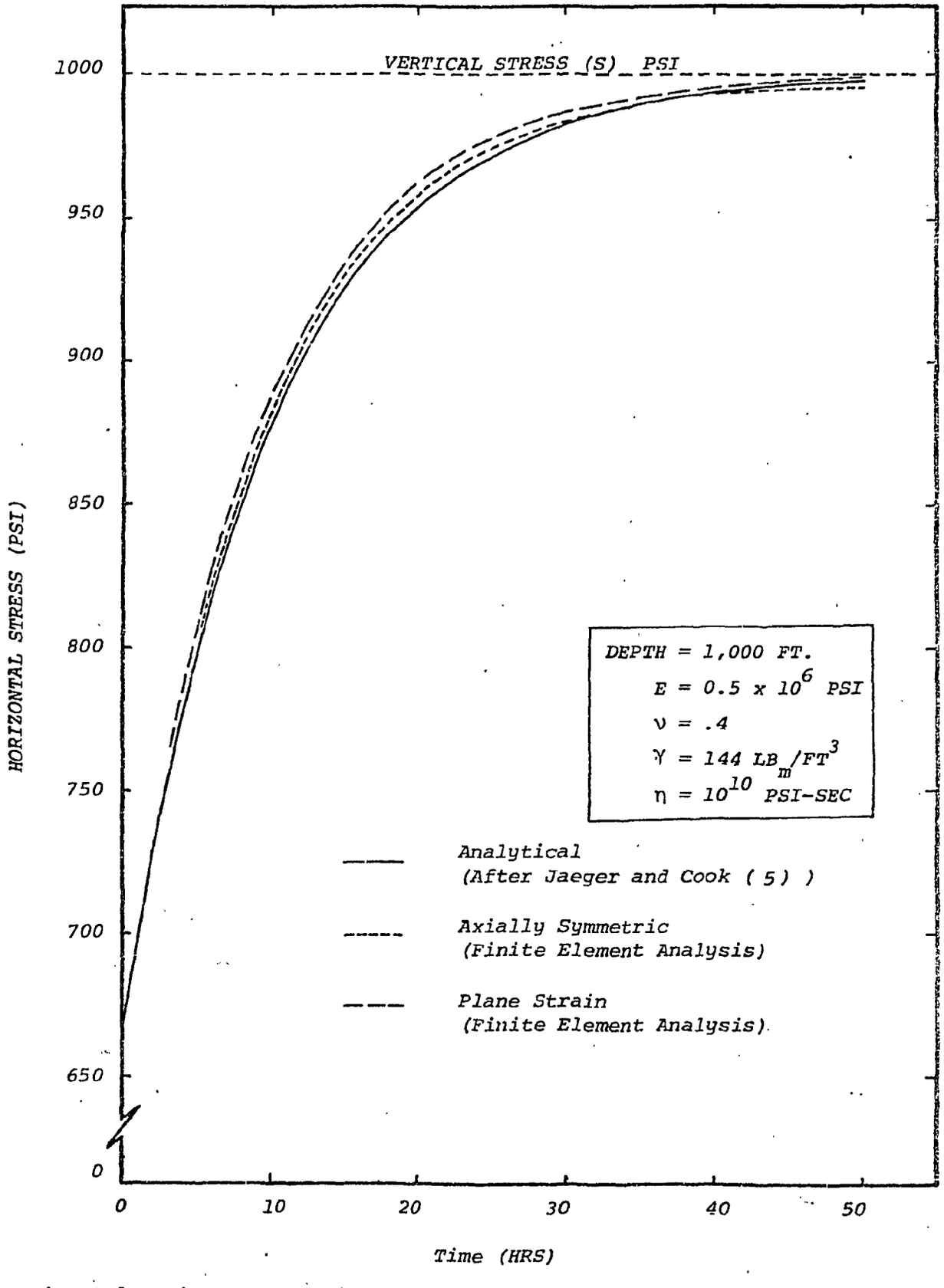

Fig. A-2. Linear Maxwellian half-space creeping from an initial elastic state toward lithostatic state.

It can be shown that the above solution holds in the plane strain case, where we have $\sigma_x = \sigma_H$. The comparison for the plane strain case is also shown in Figure A-2 again assuming a linear Maxwell model for the constitutive law.

The above comparisons illustrate the validity of the incremental approach in linear viscoelasticity problems assuming a Maxwell model. Since no solution is readily available for the empirical nonlinear creep law, the only readily available check is to reproduce the laboratory creep experiments. The curve in Figure A-3 demonstrates that the code will reproduce the average laboratory behavior.

A.4. LIMITATIONS AND DIRECTION OF FUTURE WORK

A.4.1. Limitations

Limitations of the present creep type modeling stem from the inherent assumptions discussed above, as well as from the state variable approach used to define the creep increment in any time step. From the point of view of realistic modeling of the behavior, the most severe limitations are presently the lack of plastic flow and fracture considerations in the creep code. Some work has been published where a viscoelastic-viscoplastic material model is used for salt (7); however, the model employed in this work utilized linear springs and dashpots that are not capable of modeling the nonlinear creep observed in our laboratory studies.

The state variable approach for computing strain increments is computationally convenient, but is not generally capable of accounting for the history of deformation. At this point in time, we are not able to establish the relative importance of accounting for stress history in modeling the behavior of openings in salt layers. The state variable approach is presently being used by other investigators such as Sutherland (8) and Zienkiewicz (6).

A.4.2. Direction of Future Work

Future efforts in creep modeling should be directed toward overcoming the limitations discussed above by incorporating plasticity and fracture into the creep code. In addition, experimental creep data should be used to attempt to establish a creep law in the form of heredity integrals. If such a formulation is possible, it may be necessary to store the entire

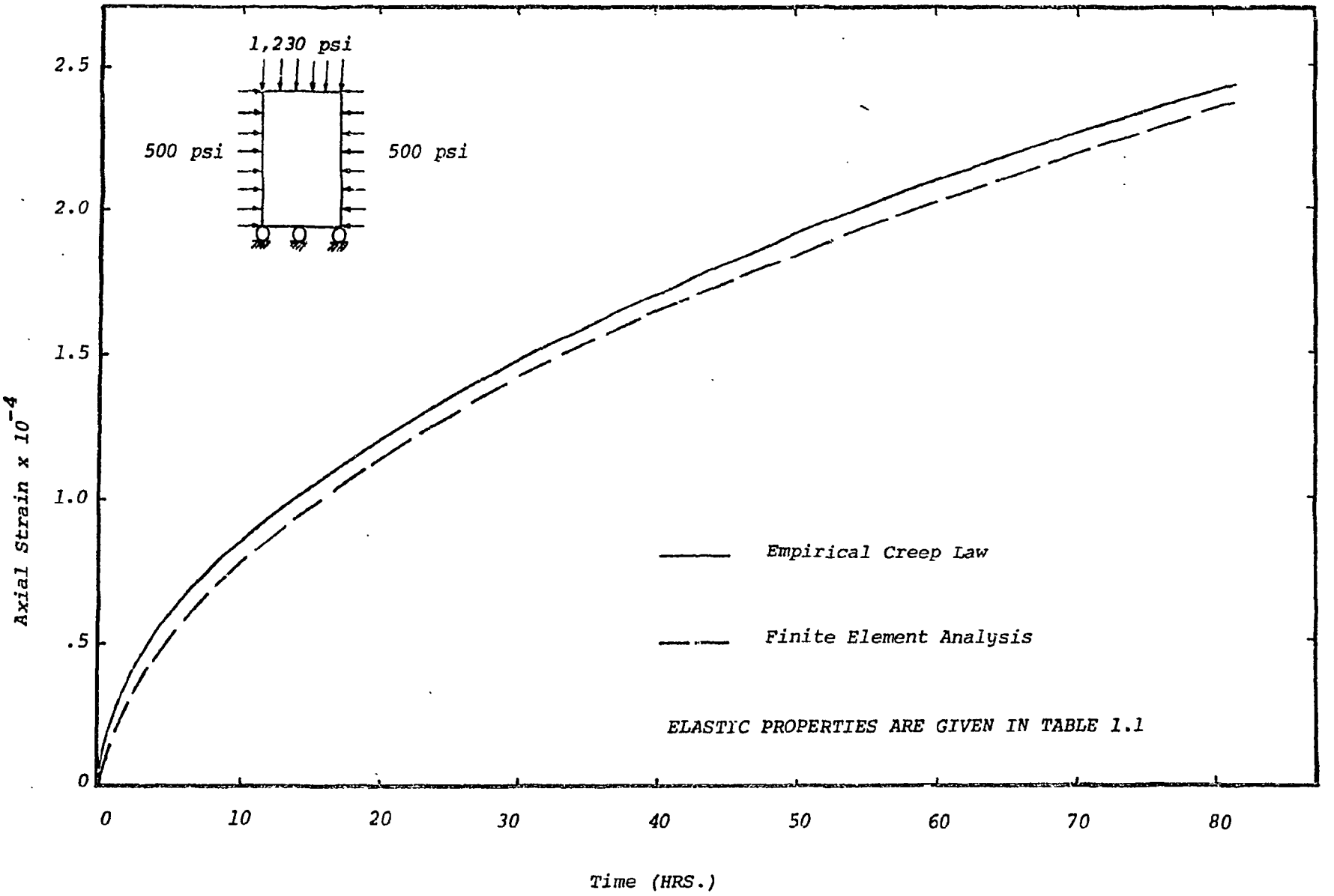

Fig. A-3. Comparison of the finite element formulation with the empirical nonlinear creep law derived from laboratory experiments.

stress history in order to be able to calculate the strain increments. This is a formidable task, but may be necessary to establish the relative importance of stress history to the behavior.

(Appendix A was prepared by James E. Russell for inclusion in Technical Memorandum Report RSI-0020)

APPENDIX B

THERMAL STRESS IN A CYLINDER WITH A CONCENTRIC CIRCULAR HOLE

B.1. Introduction

In order to provide an indication of the thermal stresses generated about the waste canister, several analytical solutions are presented herein (after Timoshenko and Goodier (1)) for cylinders having dimensions consistent with the repository model. The section of the repository considered is the general area below the room as shown in Figure B.1.

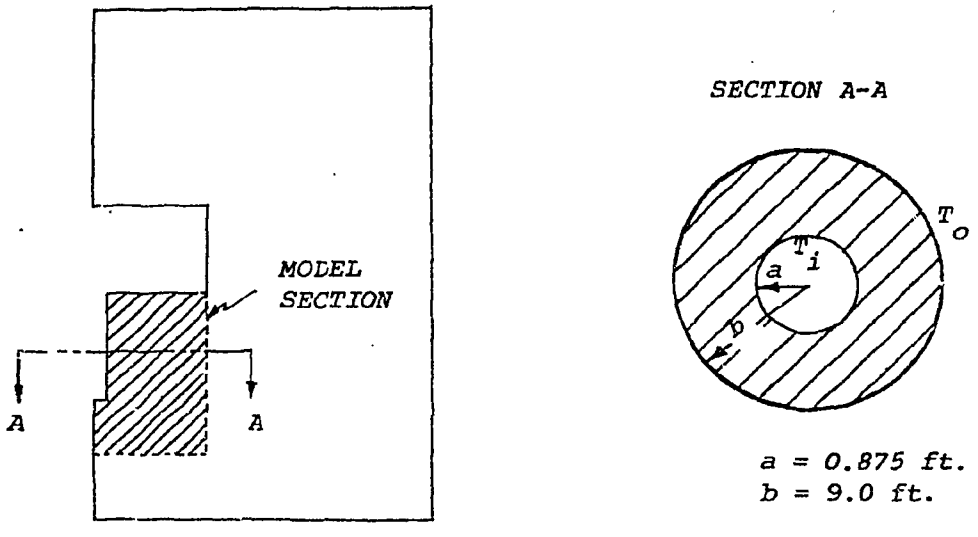

Figure B-1. Representation of the Repository for consideration as a hollow cylinder

B.2. Analytical Solutions

The inner radius of the hole in the cylinder is taken to be the radius of the drillhole, 0.875 feet. The outer boundary of the cylinder was taken at the edge of the room as a 9 foot radius. The temperature distribution is assumed to be steady state with the inner surface temperature, T_i, greater than the outer boundary temperature, T_o, which is at zero degrees Fahrenheit. As long as the temperature difference $(T_i - T_o)$ is the same, the stress results will be identical in the steady flow case. The results

presented in Figures B.2 through B.4 are for temperature differences of 100, 150, and 200 degrees Fahrenheit, respectively. Material properties utilized are the same as those presented in Section 1. The radial stress is compressive at all points and is zero at the inner and outer boundaries. The other two stress components (σ_z and σ_θ) are compressive and identical at the inner boundary, and tensile and identical at the outer boundary.

B.3. Finite Element Solutions

The model section shown in Figure B.1 is illustrated as a finite element discretization (SALT-10) in Figure B.5. The SALT-10 model is a refinement of the area below the room and around the drillhole. A temperature field equivalent to the 0.027 year temperature field utilized in the thermo/viscoelastic results presented in Section 2 was used to determine the thermoelastic results around the drillhole. A comparison of the 0.027 year temperature field - across the model at the midpoint of the waste container - and the steady state field assuming the same inner boundary temperature is illustrated in Figure B.6. The transient 0.027 year field exhibits larger thermal gradients and, consequently, larger stresses (Figure B.7) than those arising from the steady flow situation. The results in Figure B.7 were derived with both the inner and outer boundaries unrestricted. Figure B.8 illustrates the effect of restricting the boundaries against radial movement. Little change in σ_z and σ_θ is observed for the cases shown in Figure B.8, that is, assuming the drillhole free and the outer boundary fixed; and assuming both the inner and outer boundaries fixed against radial movement. The most noticeable change in comparing the three cases illustrated in Figures B.7 and B.8 is in the magnitude of the radial stress.

B.4. Conclusions

Cylindrical configurations with concentric holes heated from the inside develop stress fields of the form previously shown. In particular, the σ_z and σ_θ components are compressive at the inner boundary and tensile at the outer boundary. The radial component, σ_r, is compressive at all points and zero at the inner and outer boundaries only if these boundaries are free of tractions and displacement boundary conditions. The radial components increase in magnitude from the inner to the outer boundary with the location of the maximum value depending on the ratio of the inner surface radius to the outer surface radius. Thus, in thermally dominated problems of this type, the σ_z

and σ_θ stress components will be large and compressive near the drillhole with the radial stress reaching its maximum value away from drillhole surface. Figure B.9 illustrates the radius, r, where the magnitude of the radial stress component is largest for different inner and outer hollow cylinder radii, given by the following equation.

$$r = \sqrt{2\, C_2\, b^2}$$

where:

$$C_2 = \frac{a^2}{b^2 - a^2}\ \log_e\left(\frac{b}{a}\right)$$

a = radius of the inner surface

b = radius of the outer surface

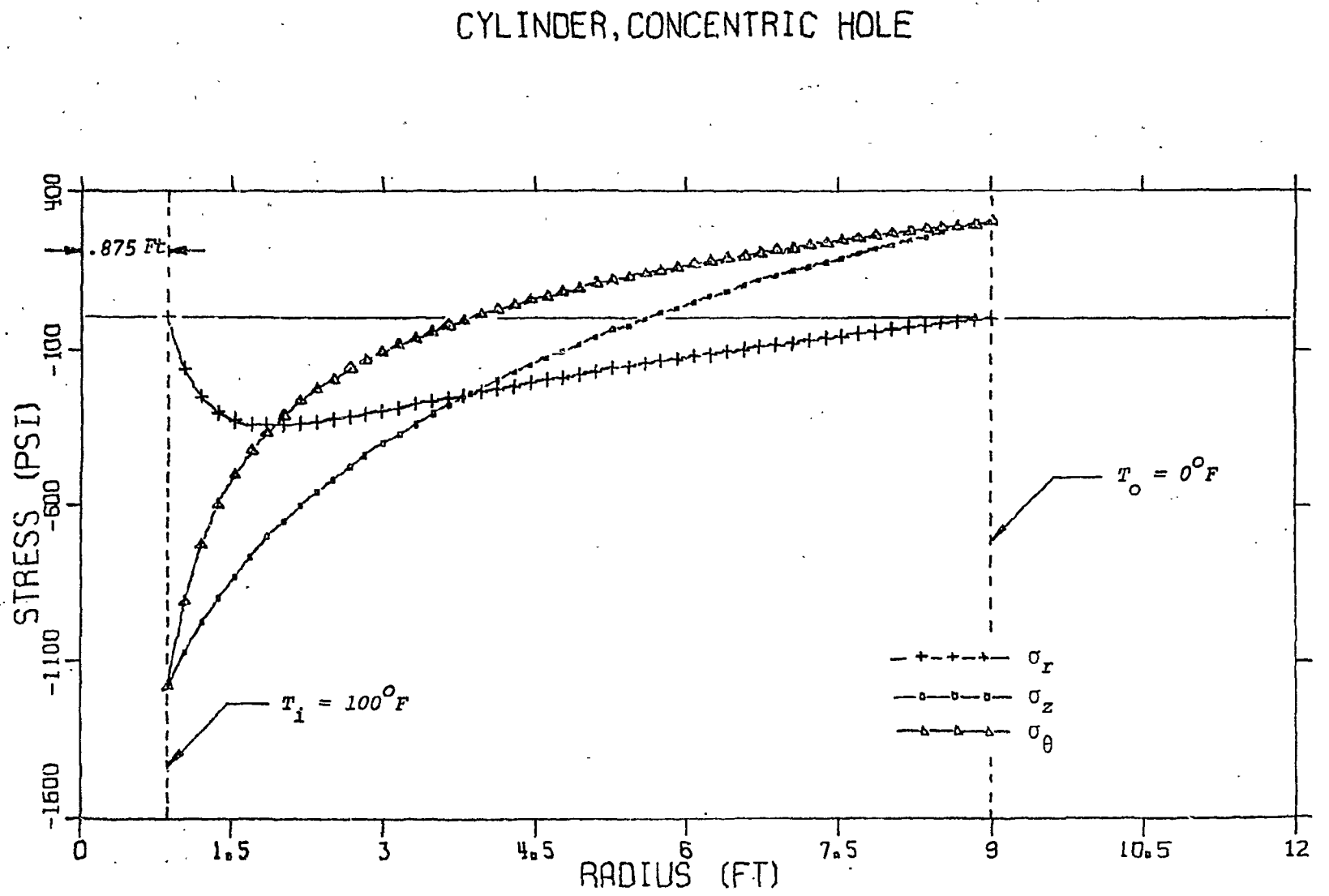

Figure B-2. Thermoelastic (Steady Heat Flow) Stresses Developed in a Cylinder with a Concentric Circular Hole for a 100°F Temperature Difference (+ Tensile).

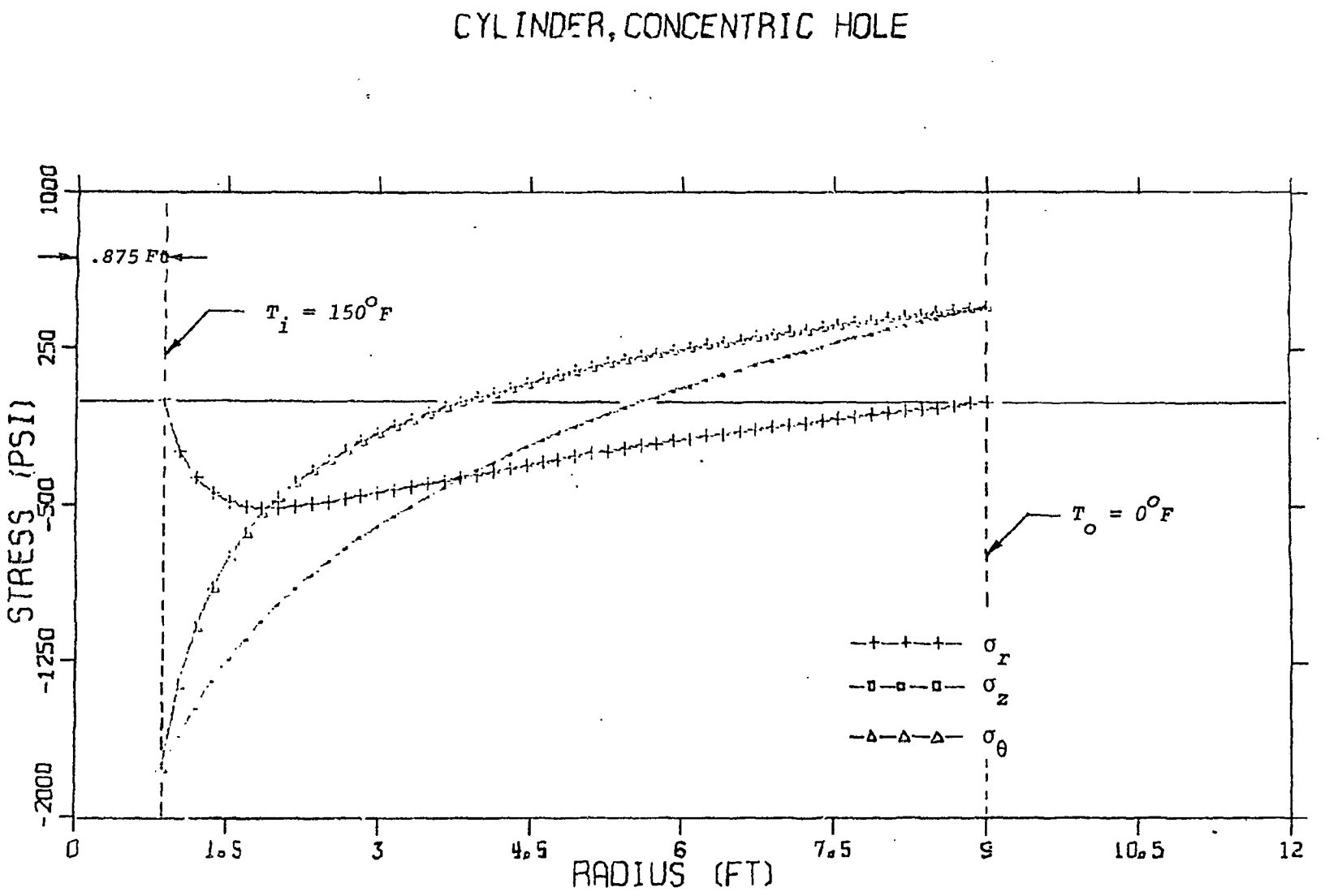

Figure B-3. Thermoelastic (Steady Heat Flow) Stresses Developed in a Cylinder with a Concentric Circular Hole for a 150°F Temperature Difference (+ Tensile).

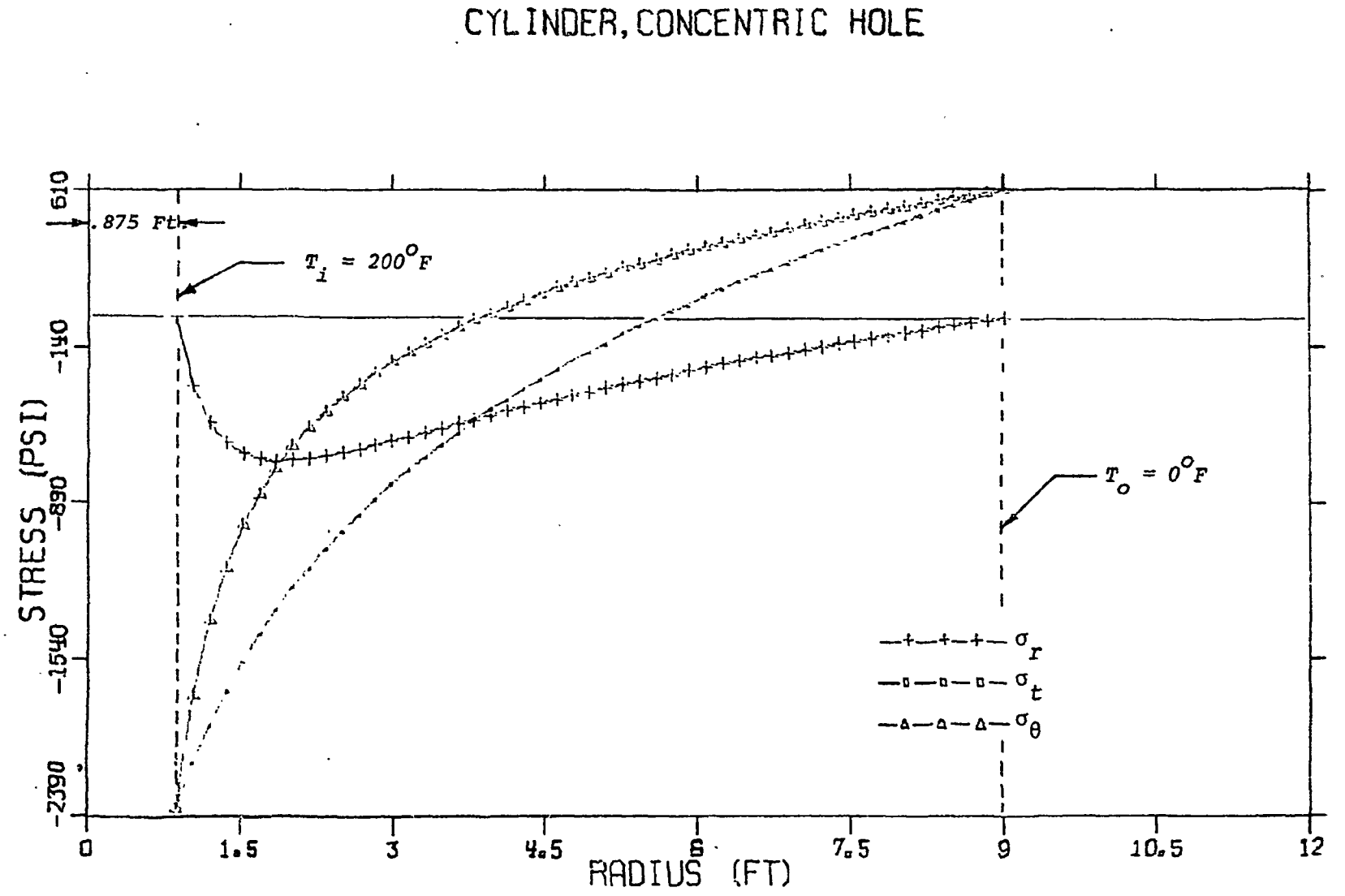

Figure B-4. Thermoelastic (Steady Heat Flow) Stresses Developed in a Cylinder with a Concentric Circular Hole for a 200°F Temperature Difference (+ Tensile).

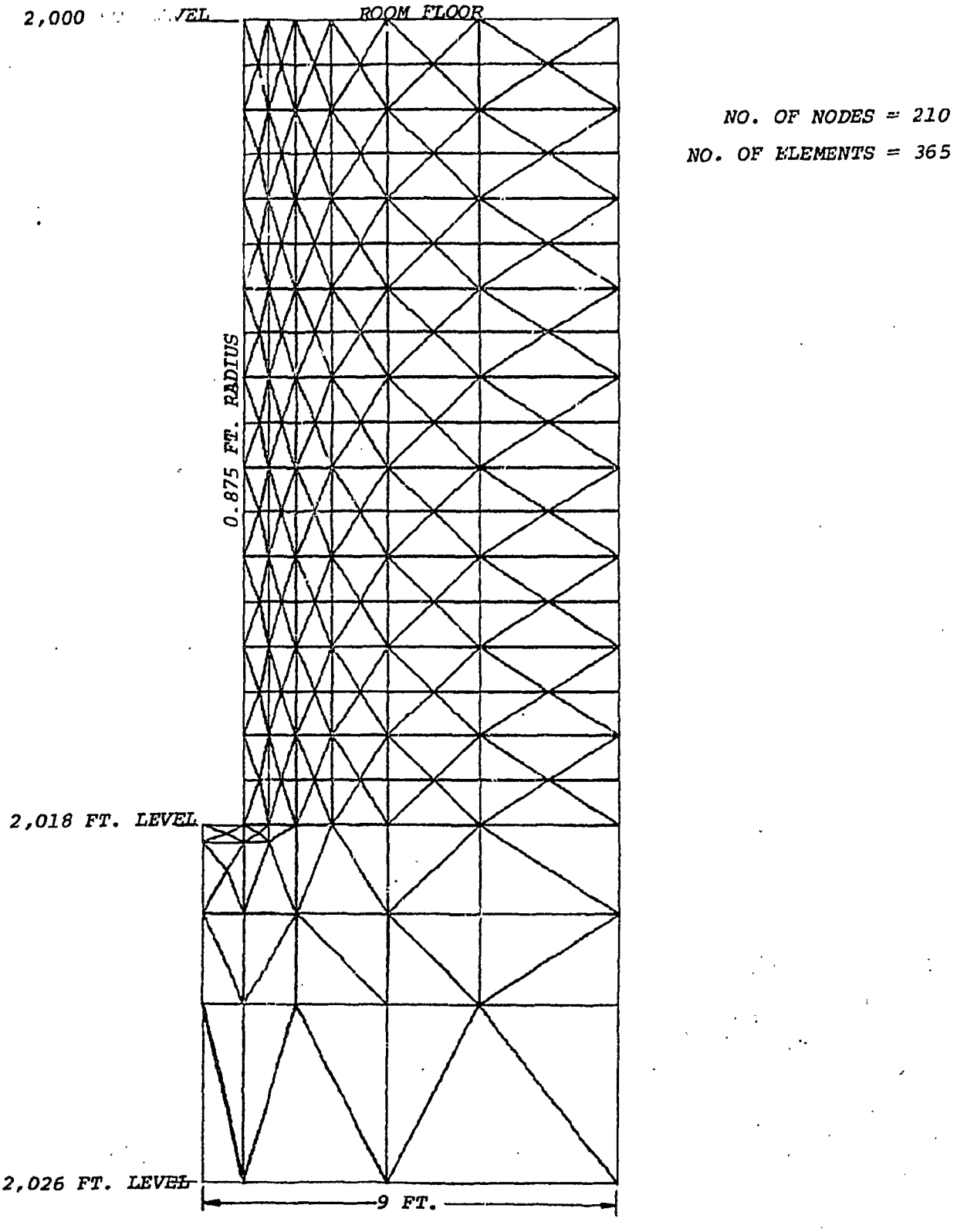

Figure B-5. Finite Element Model Utilized for Thermoelastic Analyses of the Drillhole Area.

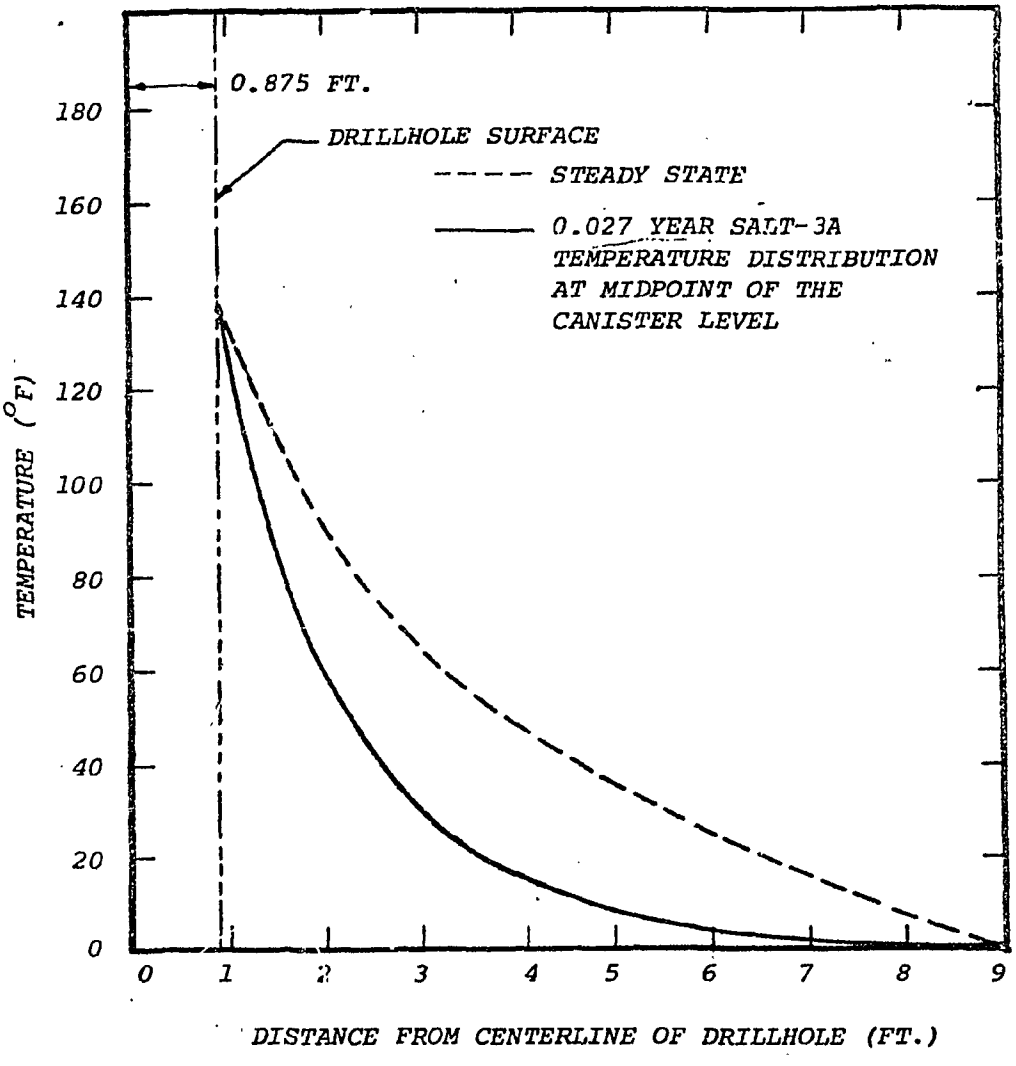

Figure B-6. Comparison of Temperature Distributions for Thermoelastic Analyses of a Cylinder with a Concentric Circular Hole.

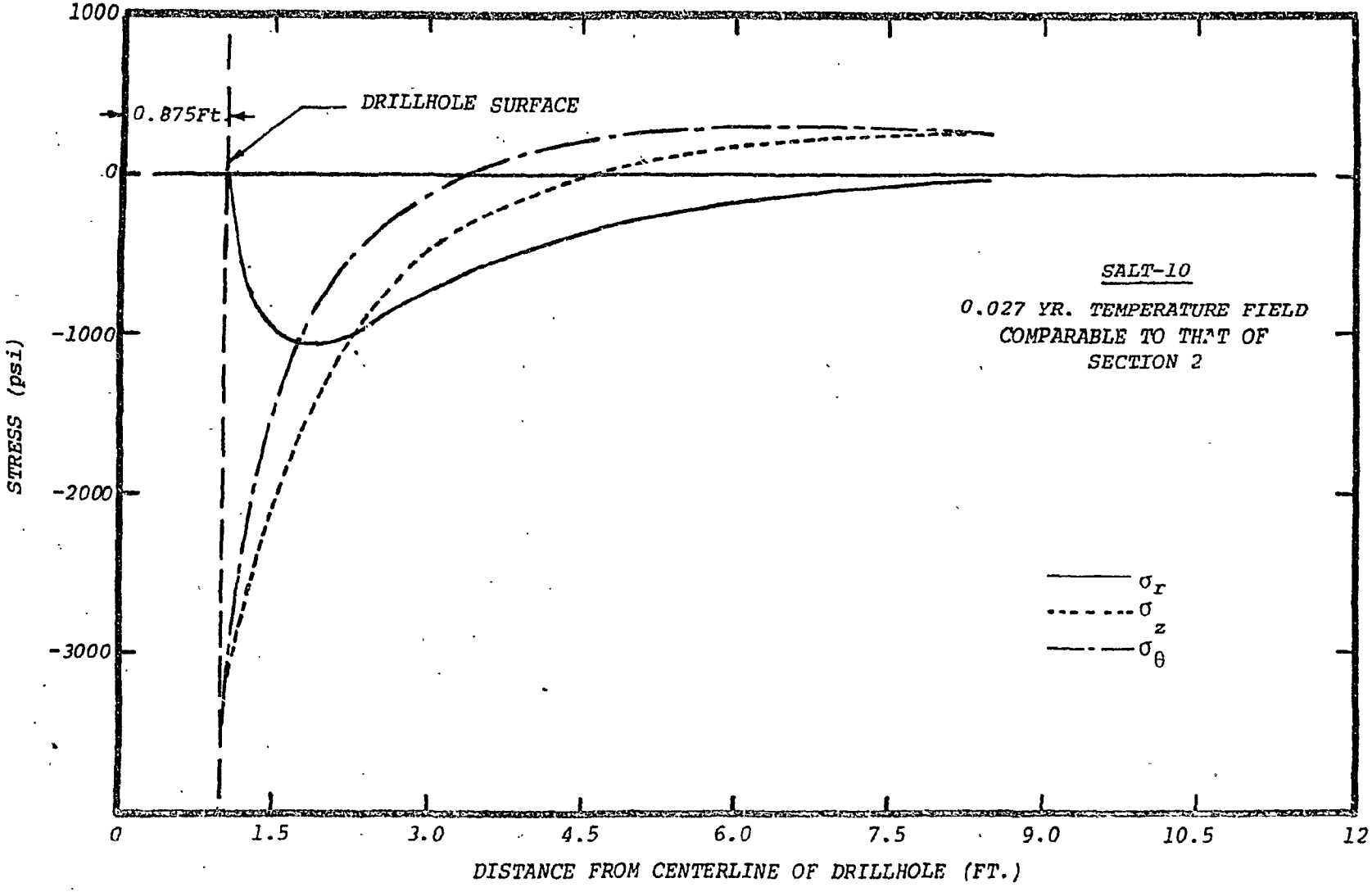

Figure B-7. Thermal Stresses Developed at the Midpoint of the Waste Container with the Inner and Outer Boundaries Unrestricted Radially (+ Tensile).

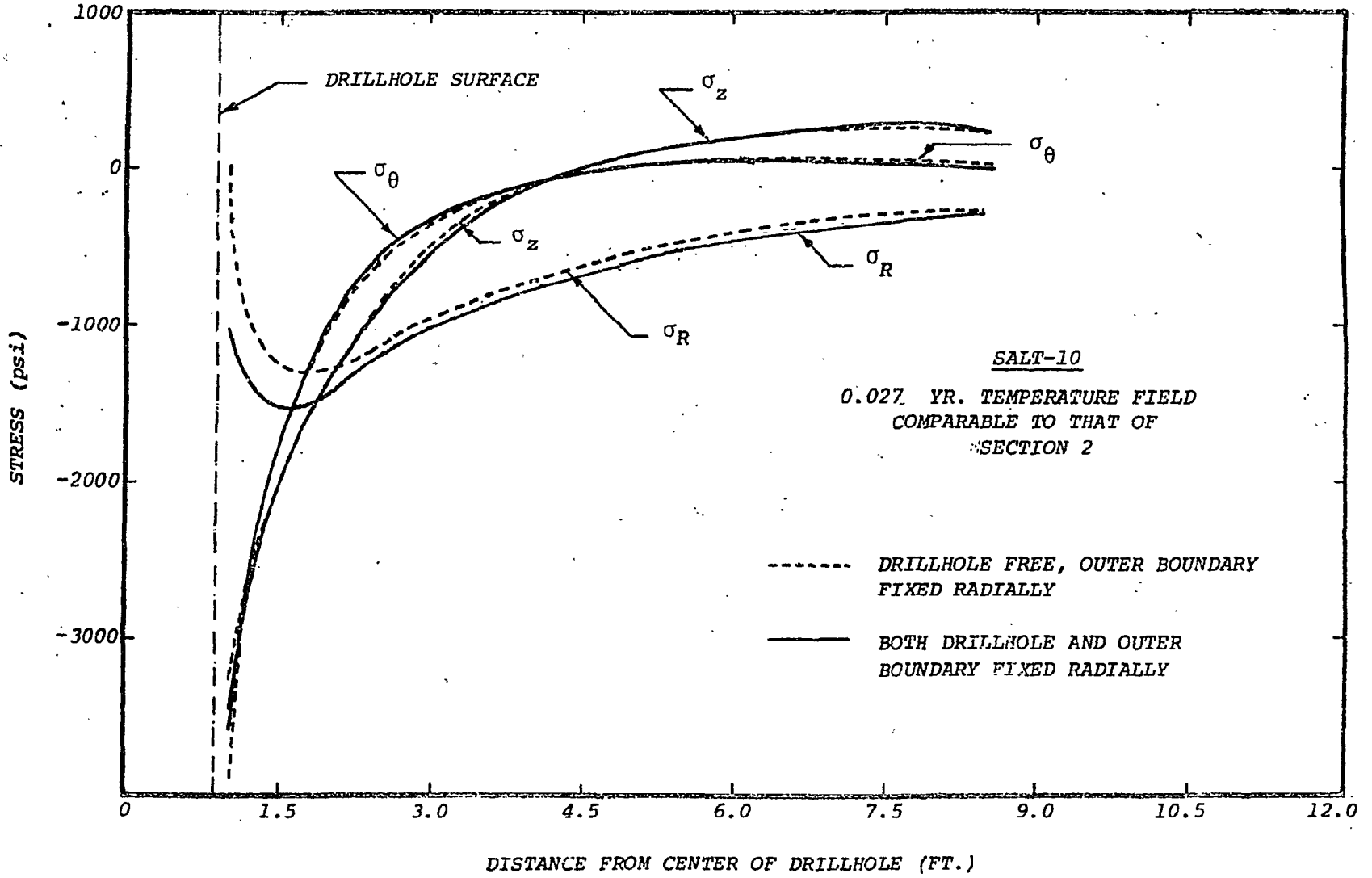

Figure B-8. Thermal Stresses Developed at the Level of the Midpoint of the Waste Container (+ Tensile).

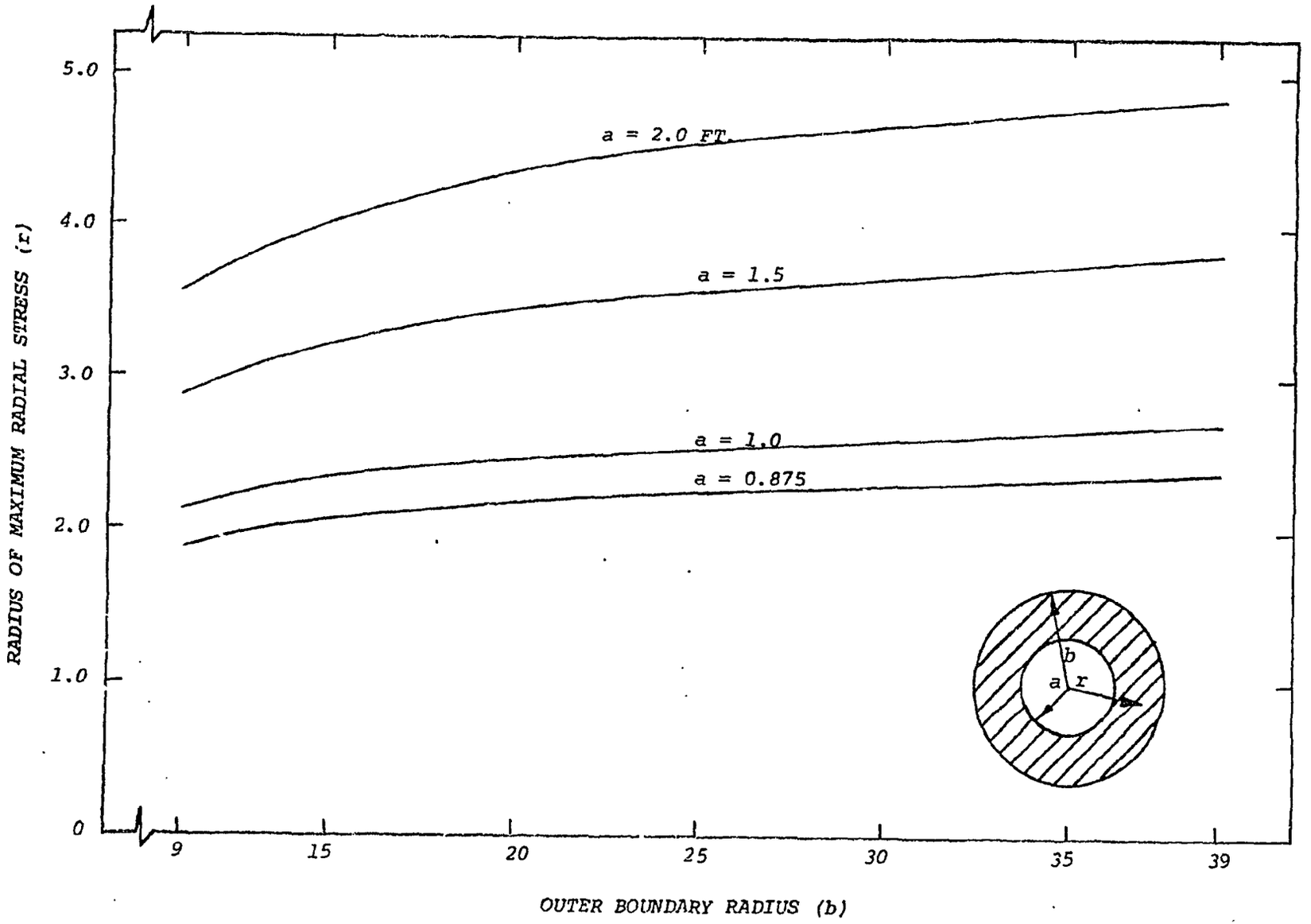

Figure B-9. Radius of the Maximum Compressive Radial Stress as a Function of Inner and Outer Radius for a Cylinder with a Concentric Circular Hole under Conditions of Steady Heat Flow.